Electric Sail Option for Cometary Rendezvous

Alessandro A. Quarta [1], Giovanni Mengali [2], Pekka Janhunen [3]

(1,2) Dipartimento di Ingegneria Civile e Industriale, University of Pisa, Italy

(3) Finnish Meteorological Institute, Finland

Abstract

The recent successes of the European Rosetta mission have shown the possibility of a close observation with one of the most evasive celestial bodies in the Solar System, the comets, and the practical feasibility of a comet rendezvous to obtain detailed information and in situ measurements. This paper discusses a preliminary study of the transfer trajectory toward the comet 67P/Churyumov-Gerasimenko (the same target used by Rosetta) for a spacecraft whose primary propulsion system is an electric solar wind sail. The use of a propellantless propulsion system with a continuous thrust is theoretically able to simplify the transfer trajectory by avoiding the need of intermediate flyby maneuvers. The problem is addressed in a parametric way, by looking for the possible optimal launch windows as a function of the propulsion system performance. The study is completed by a mass breakdown analysis of the spacecraft, for some mission scenarios of practical interest, based on the actual payload mass of the spacecraft Rosetta.

Key words: Electric solar wind sail, comet rendezvous, mission towards 67P/Churyumov-Gerasimenko

[1] Associate professor, a.quarta@ing.unipi.it. **Corresponding author**.

[2] Professor, g.mengali@ing.unipi.it.

[3] Research Manager, pekka.janhunen@fmi.fi.

Nomenclature

a	=	semimajor axis of the orbit (J2000-Ecliptic)
a_c	=	spacecraft characteristic acceleration
$\boldsymbol{a}_s$	=	E-sail propulsive acceleration
e	=	orbital eccentricity (J2000-Ecliptic)
f, g, h, k	=	modified equinoctial elements
H	=	Hamiltonian
i	=	orbital inclination (J2000-Ecliptic)
ℓ	=	tether length
L	=	true longitude
m	=	mass
M	=	mean anomaly at epoch
N	=	number of tethers
n	=	number of revolutions
p	=	semilatus rectum
r	=	Sun-spacecraft distance
t	=	time
$\boldsymbol{x}$	=	state vector
α	=	cone angle
δ	=	clock angle
$\boldsymbol{\lambda}$	=	adjoint vector
ν	=	true anomaly
τ	=	switching parameter
ω	=	argument of perihelion (J2000-Ecliptic)
Ω	=	longitude of the ascending node (J2000-Ecliptic)

Subscripts

f	=	final
i	=	initial
tether	=	single tether
tot	=	total

1 Introduction

The recent soft-landing of the robotic lander Philae [1] on the nucleus of the comet 67P/Churyumov-Gerasimenko (67P), is the realization of an ambitious and advanced space mission in which a cometary rendezvous, first in the history of the spaceflight, was completed on August 2014 by the European space probe Rosetta. The Rosetta mission is the most recent example of scientific missions towards these fascinating, and to some extent elusive, ancient bodies of our Solar System. In this context, Rosetta and its lander Philae, through in-situ measurements [2], could give interesting answers to some important questions raised by the international scientific community since many decades. Actually, the main scientific goals of Rosetta are to investigate both the origin of comets and the relationship between cometary and interstellar material. These results could be of crucial importance to obtain additional information about the origin of the Solar System and, more important, of life on Earth [3].

From the viewpoint of propellant consumption, a direct transfer towards comets using a chemical propulsion system is a very demanding option due to the high orbital eccentricity of these celestial bodies, which is often combined with a considerable orbital inclination with respect to

the Ecliptic plane. The latter point is confirmed by the data shown in Fig. 1, which illustrates the distribution of the orbital eccentricity as a function of the orbital inclination for the full set of 3321 comets [4] contained in the JPL's small-body database. Note, in particular, the considerable eccentricity of the comet 67P (about 0.641) and its non negligible orbital inclination (about 7 deg).

A typical solution to save propellant mass is to plan a mission including one or more intermediate flyby maneuvers. This approach, however, introduces a substantial complication in the transfer trajectory and causes a significant increase of the flight time due to the constraints related to the celestial bodies ephemerides. For example, in its ten years long journey to the comet, the spacecraft Rosetta exploited three gravity assists with Earth (on 2005, 2007, and 2009), and one with Mars (on 2007). The resulting trajectory also allowed the scientific probe to take two close passages with asteroids 2867 Steins (on 2008) and 21 Lutetia (on 2010).

An interesting option for saving time and propellant mass, and for avoiding the need of complex flyby maneuvers, is offered by the use of a continuous-thrust, propellantless, propulsion system such as a photonic solar sail or the more recent electric solar wind sail (E-sail). The basic idea behind the E-sail concept is to create an artificial electric field using a number of long charged tethers. Such an electric field shields the spacecraft from the solar wind ions that, impacting on it, produce a small but continuous thrust.

Even though the strength of the E-sail effect (Coulomb drag effect on charged tether or wire) has not yet been measured in space, laboratory measurements by Siguier et al. [4] around a charged wire in a flowing plasma resembling LEO conditions indicate [5] that the size of the forming electron sheath is in good agreement with earlier theoretical predictions [6]. On a technical side, a 1 km long sample of E-sail tether has been already produced [7], a lightweight Remote Unit compatible with a solar distance of 0.9-4 au is at TRL 4-5 [8] and a 100 m long

[4] See `http://ssd.jpl.nasa.gov/dat/ELEMENTS.COMET` (retrieved on 21 January 2015).

E-sail tether will fly onboard Aalto-1 CubeSat, which is scheduled to be launched into a LEO orbit in 2015 [9].

From a historical viewpoint, solar sails were originally selected as a promising option to reach a comet, starting from the mission proposed at the end of the seventies by the NASA Jet Propulsion Laboratory to rendezvous with comet 1P/Halley. The role of the solar sail concept in the Halley race is thoroughly documented in the classical textbook by Jerome Wright [10]. More recently, an interesting study regarding the solar sail capabilities is reported in a paper by Hughes and McInnes [11]. In particular, Ref. [11] points out that a solar sail mission to comet 46P/Wirtanen could reduce the launch mass by 44% (and the trip time by 68%) when compared to the original Rosetta mission scenario. Indeed, recall that Rosetta's original mission was to take a rendezvous with the comet 46P/Wirtanen in 2011, but the plan was then changed after an important failure of Ariane 5 carrier rocket.

The aim of this paper is to analyze an E-sail-based mission scenario towards comet 67P by taking into account some important characteristics of the Rosetta spacecraft. In particular, the same payload mass of Rosetta's mission has been considered to facilitate a direct performance comparison of the propulsion systems, but the same results are also applicable, at least qualitatively, to other Jupiter's families of comets. The model used to quantify the E-sail performance does not take into account the stochastic nature of the solar wind, which is known to be a high-variable plasma. Furthermore, the topological structure of the solar wind throughout the interplanetary space is different from the deterministic model used in the E-sail feasibility studies. As a result, the force field induced by the solar wind into an E-sail and applied in the following analysis should be considered as a mean value. Even though it is reasonable to expect that high-frequency fluctuation modes may be averaged by both the spacecraft inertia and the use of a suitable control law of the tethers' voltage, nevertheless more accurate models are necessary for understanding the real implication of the solar wind fluctuation on the E-sail performance. This subject is however beyond the scope of this paper.

The transfer problem is addressed in a parametric way by looking at the minimum flight time to fulfill the comet rendezvous as a function of the spacecraft characteristic acceleration a_c. The latter is defined as the maximum propulsive acceleration when the Sun-spacecraft distance is one astronomical unit. For a fixed value of a_c, the minimum flight time is initially obtained assuming an ephemeris-free model, that is, by neglecting the relative position of the celestial bodies along their own orbits. Not only this model provides the minimum transfer time (compared to the problem in which the actual planetary ephemerides are taken into account), but it also allows the optimum starting position along the Earth's heliocentric orbit to be found, as well as the optimum arrival position along the comet's heliocentric orbit.

Using the results obtained through the ephemeris-free model, the minimum-time rendezvous problem is then addressed by taking into account the ephemerides constraint, for a time interval that includes the launch dates corresponding to the optimal relative positions of the celestial bodies. Some representative values of the spacecraft characteristic acceleration are analyzed to compare the simulation results with the real flight times of the Rosetta mission. Finally, taking into account these value of a_c, the paper shows a preliminary mass breakdown analysis of an E-sail-based spacecraft, that considers a payload mass consistent with the actual value of Rosetta.

2 Simulation results with an ephemeris-free model

The optimal orbit-to-orbit heliocentric transfer is first analyzed as a function of the value of the spacecraft characteristic acceleration in the range $a_c \in [0.15,\, 1]\,\mathrm{mm/s^2}$. The E-sail trajectory can be tuned through three independent control variables, that is, τ, α and δ. The switching parameter $\tau = (0,\, 1)$ models the thruster on/off condition, and is used to account for coasting arcs in the spacecraft trajectory. The sail cone angle α is the angle between the Sun-spacecraft line and the thrust direction. The value of α can be adjusted in the range $[0,\, 30]$ deg by suitably

orienting the plane containing the sail tethers as discussed in Ref. [12]. Finally, the clock angle δ defines the orientation of the propulsive thrust in the plane perpendicular to the Sun-spacecraft direction. For all simulations it is assumed that the spacecraft is subjected to the E-sail thrust (when the propulsion system is switched on) and to the gravitational effect of the Sun only, thus neglecting any perturbation from other celestial bodies. Also, a mean field of the solar wind is assumed for all of the mission simulations . During the coasting phases, the motion is therefore Keplerian. The spacecraft is initially assumed to track an Earth heliocentric orbit. This amounts to stating that the spacecraft leaves the Earth's sphere of influence using a parabolic escape trajectory, i.e. an escape trajectory with a zero hyperbolic excess speed with respect to the planet.

In the numerical simulations, the orbital elements of Earth+Moon barycenter and comet 67P are taken from the JPL's ephemerides database, corresponding to the date of 10 August 2014, whose Modified Julian Date (MJD) is 56879. These data, which constrain the characteristics of the spacecraft osculating orbit both at the beginning and at the end of rendezvous mission, are summarized in Table 1. The optimal position of the spacecraft along the initial (Earth) and arrival (comet) heliocentric orbit, which corresponds to the solution of the minimum-time transfer problem, is an output of the optimization process. The mathematical model used to solve the optimization problem [13,14] is summarized in the Appendix .

Figure 2 shows the minimum flight times, corresponding to the ephemeris-free model, as a function of the spacecraft characteristic acceleration. In particular, Fig. 2 shows a marked dependence, with a hyperbolic-like behavior, of the flight time as a function of a_c. Note that a flight time of about ten years, comparable to that actually required by Rosetta to complete its rendezvous mission with the comet 67P, is obtained using $a_c \simeq 0.18\,\mathrm{mm/s^2}$, i.e. a moderate value of the spacecraft characteristic acceleration. The usefulness of an ephemeris-free model, when compared to a ephemeris-constrained model, is not only confined to the reduced computational time it requires. In fact, an ephemeris-free model can give interesting information

about the characteristics of the transfer orbit as, for example, the number n of full revolutions tracked by the spacecraft around the Sun during the transfer. In this sense, Fig. 2 shows that a reduction of the spacecraft characteristic acceleration implies a substantial increase of the number n, especially when the value of a_c falls below $0.3\,\mathrm{mm/s^2}$. For this reason, it is useful to ideally classify the transfer orbit within three possible families as a function of the value of n.

The first type of transfer, which will be referred to as "rapid" transfer, is characterized by the fact that the comet 67P is reached before completing a (single) full revolution around the Sun ($n = 0$). This type of transfer is obtained with a spacecraft characteristic acceleration greater than about $0.68\,\mathrm{mm/s^2}$, and it requires a flight time less than two years (or even less than one year if $a_c \geq 0.94\,\mathrm{mm/s^2}$). An example of rapid transfer trajectory with a flight time of about 340 days is drawn in Fig. 3, which shows the ecliptic projection of the optimal trajectory when $a_c = 1\,\mathrm{mm/s^2}$. Note that all of the transfers studied in this paper are fully three-dimensional even if, for the sake of visualization, the figures show the ecliptic projection of the spacecraft heliocentric trajectories.

On the other hand, a mission that requires a number of revolutions $n \geq 3$ is referred to as "slow" transfer. Taking into account Fig. 2, such a transfer is obtained when the spacecraft characteristic acceleration is less than about $0.28\,\mathrm{mm/s^2}$. In this case the flight time is greater than six years and its length quickly increases as a_c is decreased. The slow transfers are characterized by involved spacecraft trajectories in which the propulsion system is switched off or on many times, so that a number of coasting arcs take place. The accurate numerical simulation of those trajectories is rather difficult and is computationally very expensive, especially due to the fact that the solution of the two-point boundary value problem associated to the optimal transfer is highly sensitive to the unknown (initial) variables to be found.

Finally, the intermediate case, in which $n = \{1, 2\}$, is referred to as "moderate" transfer. In this case the flight times are between two and six years, and the spacecraft characteristic

accelerations are roughly in the range $a_c \in [0.28, 0.68]\,\mathrm{mm/s^2}$. The analysis of those trajectories is much simpler than in the case of slow transfers, partly because the number of coasting phases is small (i.e., not exceeding two or three). To summarize, the shape of the spacecraft trajectory (and, in particular, the number of full revolutions) is strongly dependent on the value of the spacecraft characteristic acceleration, as is clearly shown in Fig. 4, which illustrates six trajectories obtained with different values of a_c. Note that the meaning of the symbols appearing in the trajectories of Fig. 4 is described in Fig. 3.

The previous classification according to the three transfer types (i.e. slow, moderate and rapid), is rather arbitrary even if a similar nomenclature was adopted by the Authors in another study [15] involving a mission analysis toward a near-earth asteroid. However, this nomenclature is particularly useful to give a meaningful and direct description of the simulation times necessary to obtain the optimal trajectories. For example, the time required to simulate a slow transfer is about an order of magnitude (in some cases even two orders of magnitude) greater than that required for a rapid transfer.

It is interesting to note that, according to Fig. 4, the optimal transfer in the ephemeris-free model is characterized by a final true anomaly (i.e. a spacecraft's true anomaly on the comet's heliocentric orbit at rendezvous) that is nearly independent of the value of a_c. Such a true anomaly value is about $\nu_f \simeq 140\,\mathrm{deg}$ which, taking into account the comet's orbital data summarized in Table 1, implies that the Sun's distance at rendezvous is roughly $r_f \simeq 4\,\mathrm{au}$. This is an useful result, because one important constraint of Rosetta mission is related to the rendezvous distance [16], which must take place at a Sun's distance less than 4.4 au. Another mission constraint [16] states that the spacecraft shall support full science operation at a distance not less than 3.25 au from the Sun. From this viewpoint an orbital rendezvous that takes place when the comet is going away from its perihelion (see the black squares in Fig. 4), is advantageous.

The flight times and the characteristics of the transfer orbit, which are detailed in Fig. 2 and Table 2, should be considered as a first approximation only of the actual results that can be found by taking into account the real position of the celestial bodies (i.e. the Earth at departure and the comet at rendezvous) along their own orbits. In this sense, these results represent the starting point for a more accurate analysis with ephemeris-constrained data, which is the topic of the next section.

3 Simulation results with an ephemeris-constrained model

When the actual positions of the two celestial bodies along their own orbits are taken into account, the optimal launch date and the corresponding optimal trajectory can be calculated with the following approach. For a given value of spacecraft characteristic acceleration, Table 2 provides the minimum time interval (Δt) and the spacecraft true anomaly along the Earth's heliocentric orbit at departure (ν_i) and along the comet's orbit at rendezvous (ν_f). Using the orbital data of Table 1, that is, the position of the two celestial bodies on 10 August 2014, and solving a classical Kepler problem, it is possible to find the best departure date at which the actual position of the two celestial bodies is closest to the spatial configuration of the ephemeris-free model. For a near-term mission, the best departure date has been calculated within a time range of ten years, from the 1st January 2015 to the 1st January 2025.

When the best departure date is known, the constrained minimum flight time is found starting from the actual Earth's position at the departure date, and enforcing the final spacecraft (heliocentric) position to coincide with the actual position of the comet at the rendezvous date. This method may be applied to all values of the spacecraft characteristic acceleration within the range used in the preliminary analysis with the ephemeris-free model. Three different mission scenarios will now be discussed according to the three different cases of slow, moderate and rapid transfer.

3.1 Slow transfer

In this first case study, the spacecraft characteristic acceleration is assumed to be $0.2\,\mathrm{mm/s^2}$. Table 2 shows that the minimum flight time in an ephemeris-free model is 3149 days (about 8.63 years) and, during the transfer, the spacecraft completes four revolutions around the Sun. In particular, the topology of the transfer trajectory is close to that illustrated in Fig. 4 with $a_c = 0.18\,\mathrm{mm/s^2}$.

When the constraint due to ephemerides is taken into account, the best departure date is 14 October 2020. In that case the flight time is 3164 days (only 0.5% greater than the minimum, ephemeris-free, value), and the rendezvous takes place at a Sun's distance of 3.44 au, when the true anomaly is about 130 deg. This result is illustrated in Fig. 5, which shows the spacecraft (constrained) optimal transfer trajectory.

The use of a propulsion system with a continuous thrust allows a certain flexibility to be obtained in the departure date. In this respect, a possible shift of the departure date, compared to the nominal value of 14 October 2020, implies an increase of the total flight time. Nevertheless, such an increase is rather small, in percentage terms, even if the departure date is either advanced or delayed by some weeks. This is confirmed by the results of Fig. 6, which shows the sensitivity of the flight time as a function of the departure date, using a time interval of three months around the nominal date of 14 October 2020. For example, by delaying the departure date of one and half month (thus starting on the 1$^{\mathrm{st}}$ December 2020), the minimum flight time would be 3225 days, which means a transfer time increase less than 2% with respect to the optimal value of 3164 days.

Figure 7 shows the distance from the Sun at rendezvous r_f as a function of the departure date, when $a_c = 0.2\,\mathrm{mm/s^2}$. Note that the value of r_f is always less than the maximum distance (4.4 au) imposed by the mission requirements for Rosetta [16]. In this case the final

Sun's distance presents a more pronounced variation with the departure date. For example, a departure date on 1st December 2020 corresponds to a Sun's distance of 4.04 au, with an increase of about 17% with respect to the value that can be obtained when the nominal (i.e. the best) departure date is selected.

3.2 Moderate transfer

In this case the value of the spacecraft characteristic acceleration is set equal to $0.4\,\mathrm{mm/s^2}$. Using the data of Table 2, the ephemeris-free model states that the minimum flight time is 1357 days, i.e. about 3.71 years. Accordingly, the ephemeris-constrained model suggests an optimal departure date on 15 July 2019. In that case the comet 67P can be reached within a flight time of about 1359 days, nearly coinciding with that of the ephemeris-free model. The optimal trajectory completes one revolution around the Sun, as is shown in Fig. 8.

In terms of performance sensitivity to the departure date, Fig. 9 shows that a delay of few weeks corresponds to a flight time increase of about one hundred days. An earlier launch, instead, does not affect substantially the total flight time, because a departure on 1st June 2019 implies, for example, that the comet 67P is reached in less than 1400 days. Moreover, the Sun-spacecraft distance at rendezvous is between 3.9 au and 4.6 au, see Fig. 10. In particular, the distance corresponding to the optimal departure date is $r_f \simeq 3.95$ au, a value compatible with the mission requirements of Rosetta. The constraint on the final distance tends to reduce the admissible launch window. Indeed, Fig. 10 shows that a departure beyond 15 August 2019 implies a final distance from the Sun exceeding the limit of 4.4 au.

3.3 Rapid transfer

For the rapid transfer case, the example value of the spacecraft characteristic acceleration is $a_c = 1\,\mathrm{mm/s^2}$. Adopting the same nomenclature used for a photonic solar sails [17], $a_c = 1\,\mathrm{mm/s^2}$ is usually referred to as "canonical" value, as it is usually the reference value used to quantify the mission performance in a given mission scenario. Recalling from Table 2 that the ephemeris-free model provides a minimum flight time of 340 days, and a true anomaly at departure (arrival) of about 250 deg (112 deg), the previously described procedure states that the best departure date is on 3 September 2021. Starting from that date, the flight time with ephemerides constraint is 393 days, which corresponds to an increase of about 15% compared to the value shown in Table 2. This increase is, in percentage terms, much higher than that obtained in the two preceding cases and is probably due to the insufficient length of the time interval within which the best departure date is sought. Moreover, a high value of the spacecraft characteristic acceleration implies that the flight times are moderate (about one year) and the introduction of a constraint on the ephemerides has a strong effect on the total flight time. The transfer trajectory is drawn in Fig. 11, which is similar to that obtained for an ephemeris-free model and illustrated in Fig. 3.

The parametric analysis of the sensitivity to the departure date is shown in Fig. 12, which involves a time range of two months around the nominal departure date. The figure shows the existence of a marked sensitivity to the departure date (in particular for a delayed launch), which implies a flight time increase of more than one hundred days. In all of the analyzed cases the Sun's distance at rendezvous is always less than the maximum value of 4.4 au, as is shown in Fig. 13. Moreover, the rendezvous always takes place when the comet is moving away from the Sun, that is, when the true anomaly is less than 180 deg. In the optimal case the final distance is $r_f \simeq 2.85\,\mathrm{au}$ and the corresponding true anomaly is $\nu_f \simeq 116\,\mathrm{deg}$.

4 Spacecraft main characteristics

Having found the transfer performance in terms of optimal flight times and the best departure dates as a function of the value of a_c, it is now interesting to analyze the main characteristics of the E-sail-based spacecraft. To this end, a preliminary spacecraft mass breakdown analysis was performed using a parametric and semi-analytical model, originally discussed in Ref. [18], whose main input performance parameter is given by the spacecraft characteristic acceleration. In particular, the auxiliary tethers are assumed to be made of 7.6 μm thin Kapton, whereas the nominal tether voltage is set equal to 25 kV. For comparative purposes, the same payload mass used in the Rosetta spacecraft is assumed, that is, a total payload mass of 265 kg, comprising 165 kg of science payload and 100 kg of lander [19].

Taking into account the results from the previous section, the representative values of spacecraft characteristic acceleration are chosen to be $a_c = \{0.2,\, 0.4,\, 1\}\,\mathrm{mm/s^2}$, which correspond to the cases of slow, moderate and rapid transfers. The results are summarized in Table 3 for mission scenarios with and without the lander.

For each pair of payload mass and spacecraft characteristic acceleration, Table 3 shows the required total E-sail tether length ℓ_{tot}, the total mass of the spacecraft including a 20 % uncertainty margin, the number of tethers N, the length of each tether ℓ_{tether}, and the optimal ephemeris-free flight time (see also Table 2). Note that values in Table 3 are calculated without including the mass of a conventional propulsion system required by the probe to fly around the comet in a controlled way, because the E-sail is not necessarily agile enough for such a task. Table 3 shows that, even in the challenging case in which the lander is included and the spacecraft characteristic acceleration is $1\,\mathrm{mm/s^2}$, a solution exists with a reasonable value of in-flight total mass of about 820 kg. Also, a spacecraft without a lander and a mission with a moderate value of flight time (for example, 3.7 years), requires a total mass of 470 kg and about

28 tethers of 11 km length each. Finally, Table 3 summarizes the main spacecraft characteristics for a hypothetical mission with a (small) payload mass of 30 kg. Note that a scientific payload mass value on the order of 10 kg − 20 kg is consistent with other studies for a rendezvous mission with a near-Earth asteroid using a solar sail-based spacecraft [20]. In that case, a rapid transfer would require a total in-flight mass of 130 kg and 24 tethers of 9.4 km length each.

5 Discussion and conclusions

The capability of providing a continuous propulsive acceleration, for a prolonged time interval and without the need of propellant, makes an E-sail an interesting option for missions toward minor celestial bodies such as the comets. An analysis of a mission scenario involving a rendezvous mission to the comet 67P/Churyumov-Gerasimenko has shown that an E-sail-based spacecraft with medium-low performance is able to reach this celestial body with transfer times comparable to that of the European Rosetta mission. However, significantly shorter flight times can be obtained with an E-sail with medium-high performance, i.e. with a spacecraft characteristic acceleration of about one millimeter per square seconds.

Assuming a scientific payload mass of 30 kg and a spacecraft characteristic acceleration of about 0.4 mm/s^2, the optimal ephemeris-free flight time is 3.7 years and the propulsion system requires 12 tethers only of 6.1 km length each. In that case, the total in-flight mass is 105 kg including a 20 % margin. This preliminary mission analysis indicates that if future E-sail experimental tests were to show the basic properties investigated so far (and mentioned in the Introduction), then the E-sail propulsion would become a very useful tool also for cometary rendezvous missions like the Rosetta mission.

An interesting extension of this work involves the possibility of widening the space mission, including an Earth return phase. As a matter of fact, since no propellant is required by the

spacecraft, the only condition for the return phase fulfillment is that the vehicle has to wait until a suitable reentry window opens. Such a mission extension would theoretically guarantee not only an in situ analysis of the comet, but also the possibility of transferring to Earth some samples taken from the comet's surface. Another extension of the work involves the use of a fleet of smaller E-sail-based spacecraft, which could be used to study different targets with the aim of performing more limited tasks, such as measuring some isotope ratios of different celestial bodies.

Appendix

This Appendix summarizes the mathematical model used for simulating the optimal trajectories discussed in the paper. The E-sail equations of motion are written in terms of modified equinoctial elements $\{p,\ f,\ g,\ h,\ k,\ L\}$ while the time scale used for the numerical integration of the equations is the JPL ephemeris time argument $\mathrm{T_{eph}}$. The compact form of equations of motion is

$$\dot{\boldsymbol{x}} = A\,\boldsymbol{a}_s + \boldsymbol{c}$$

where $\boldsymbol{a}_s$ is the E-sail propulsive acceleration and $\boldsymbol{x}$ is the vector of modified equinoctial elements, defined as

$$\boldsymbol{x} \triangleq [p,\ f,\ g,\ h,\ k,\ L]^{\mathrm{T}}$$

Also

$$\boldsymbol{c} \triangleq \left[0,\ 0,\ 0,\ 0,\ 0,\ \sqrt{\mu_\odot\, p}\,\left(\frac{1+f\,\cos L+g\,\sin L}{p}\right)^2\right]^{\mathrm{T}}$$

and $A \in \mathbb{R}^{6\times 3}$ is a suitable matrix whose generic entry is referred to as A_{ij}. In particular, $A_{11} = A_{13} = A_{41} = A_{42} = A_{51} = A_{52} = A_{61} = A_{62} = 0$, while

$$A_{12} = \frac{2\,p}{1 + f\,\cos L + g\,\sin L}\sqrt{\frac{p}{\mu_\odot}}$$

$$A_{21} = \sin L\sqrt{\frac{p}{\mu_\odot}}$$

$$A_{22} = \frac{(2 + f\,\cos L + g\,\sin L)\,\cos L + f}{1 + f\,\cos L + g\,\sin L}\sqrt{\frac{p}{\mu_\odot}}$$

$$A_{23} = -\frac{g\,(h\,\sin L - k\,\cos L)}{1 + f\,\cos L + g\,\sin L}\sqrt{\frac{p}{\mu_\odot}}$$

$$A_{31} = -\cos L\sqrt{\frac{p}{\mu_\odot}}$$

$$A_{32} = \frac{(2 + f\,\cos L + g\,\sin L)\,\sin L + g}{1 + f\,\cos L + g\,\sin L}\sqrt{\frac{p}{\mu_\odot}}$$

$$A_{33} = \frac{f\,(h\,\sin L - k\,\cos L)}{1 + f\,\cos L + g\,\sin L}\sqrt{\frac{p}{\mu_\odot}}$$

$$A_{43} = \frac{(1 + h^2 + k^2)\,\cos L}{2\,(1 + f\,\cos L + g\,\sin L)}\sqrt{\frac{p}{\mu_\odot}}$$

$$A_{53} = \frac{(1 + h^2 + k^2)\,\sin L}{2\,(1 + f\,\cos L + g\,\sin L)}\sqrt{\frac{p}{\mu_\odot}}$$

$$A_{63} = \frac{h\,\sin L - k\,\cos L}{1 + f\,\cos L + g\,\sin L}\sqrt{\frac{p}{\mu_\odot}}$$

The components of the propulsive acceleration $\boldsymbol{a}_s$ in a classical radial-tangential-normal reference frame $\mathcal{T}$ are

$$[\boldsymbol{a}_s]_{\mathcal{T}} = \tau\,a_c\left(\frac{r_\oplus}{r}\right)\,[\cos\alpha,\ \sin\alpha\cos\delta,\ \sin\alpha\sin\delta]^{\mathrm{T}}$$

where $r_\oplus = 1\,\mathrm{au}$, while the Sun-spacecraft distance r can be written in terms of modified equinoctial elements as

$$r = \frac{p}{1 + f\,\cos L + g\,\sin L} \tag{1}$$

The problem discussed in section 2 consists of finding the control law $\boldsymbol{u}(t)$, where $\boldsymbol{u} \triangleq [\alpha,\, \delta,\, \tau]^{\mathrm{T}}$ that maximizes the performance index $J \triangleq -t_f$, where t_f is the flight time necessary to transfer the spacecraft from an initial $\boldsymbol{x}_0$ to a final $\boldsymbol{x}_f$ prescribed state. The Hamiltonian of the system is

$$H \triangleq (A\,\boldsymbol{a}_s) \cdot \boldsymbol{\lambda} + \boldsymbol{c} \cdot \boldsymbol{\lambda} \tag{2}$$

where $\boldsymbol{\lambda} \triangleq [\lambda_p,\ \lambda_f,\ \lambda_g,\ \lambda_h,\ \lambda_k,\ \lambda_L]^{\mathrm{T}}$ is the adjoint vector whose time derivative is given by the Euler-Lagrange equation:

$$\dot{\boldsymbol{\lambda}} = -\frac{\partial H}{\partial \boldsymbol{x}} \tag{3}$$

The explicit expression of the Euler-Lagrange equation is rather involved and is not reported here for the sake of conciseness. The optimal value of the control variables α, δ and τ is obtained by maximizing, at any time, the Hamiltonian H. For example, by enforcing the necessary condition $\partial H/\partial \delta = 0$, the optimal control law for the clock angle δ is:

$$\sin\delta = A_{23}\,\lambda_f + A_{33}\,\lambda_g + A_{43}\,\lambda_h + A_{53}\,\lambda_k + A_{63}\,\lambda_L \tag{4}$$

$$\cos\delta = A_{32}\,\lambda_g + A_{12}\,\lambda_p + A_{22}\,\lambda_f \tag{5}$$

Likewise, $\partial H/\partial \alpha = 0$ and $\partial H/\partial \tau = 0$ can be solved for obtaining the control laws of α and τ. The two-point boundary-value problem associated to the variational problem is constituted by the 6 scalar equations of motion and by the 6 scalar Euler-Lagrange equations. The corresponding 12 boundary conditions are related to the desired spacecraft position and velocity at the initial ($t = 0$) and final ($t = t_f$) time. In particular, the boundary conditions for the

ephemeris-free model are

$$p(0) = p_\oplus, \quad f(0) = f_\oplus, \quad g(0) = g_\oplus, \quad h(0) = h_\oplus, \quad k(0) = k_\oplus, \quad \lambda_L(0) = 0 \tag{6}$$

$$p(t_f) = p_\diamond, \quad f(t_f) = f_\diamond, \quad g(t_f) = g_\diamond, \quad h(t_f) = h_\diamond, \quad k(t_f) = k_\diamond, \quad \lambda_L(t_f) = 0 \tag{7}$$

where subscript $\diamond$ corresponds to the target comet 67P. The transversality condition $H(t_f) = 1$ is finally used to obtain the (optimal) value of t_f.

References

[1] S. Ulamec, J. Biele, A. Blazquez, B. Cozzoni, C. Delmas, C. Fantinati, P. Gaudon, K. Geurts, E. Jurado, O. Küchemann, V. Lommatsch, M. Maibaum, H. Sierks, L. Witte, Rosetta lander - Philae: Landing preparations, Acta Astronautica 107 (2015) 79–86, doi: 10.1016/j.actaastro.2014.11.019.

[2] S. Ulamec, J. Biele, P.-W. Bousquet, P. Gaudon, K. Geurts, T.-M. Ho, C. Krause, C. Lange, R. Willnecker, L. Witte, Landing on small bodies: From the Rosetta lander to MASCOT and beyond, Acta Astronautica 93 (2014) 460–466, doi: 10.1016/j.actaastro.2013.02.007.

[3] J. Oró, A. Lazcano, P. Ehrenfreund, Comets and the Origin and Evolution of Life, 2nd Edition, Springer, 2006, Ch. 1, pp. 1–18.

[4] J. Siguier, P. Sarrailh, J. Roussel, V. Inguimbert, G. Murat, J. SanMartin, Drifting plasma collection by a positive biased tether wire in LEO-like plasma conditions: current measurement and plasma diagnostics, IEEE Transactions on Plasma Science 41 (12) (2013) 3380–3386, doi: 10.1109/TPS.2013.2257871.

[5] P. Janhunen, Coulomb drag devices: Electric Solar Wind Sail propulsion and ionospheric deorbiting, Space Propulsion 2014, Köln, Germany, 2014, paper SP2014_2969331, Session 80.

[6] P. Janhunen, Increased electric sail thrust through removal of trapped shielding electrons by orbit chaotisation due to spacecraft body, Annales Geophysicae 27 (8) (2009) 3089–3100, doi:

10.5194/angeo-27-3089-2009.

[7] H. Seppänen, T. Rauhala, S. Kiprich, J. Ukkonen, M. Simonsson, R. Kurppa, P. Janhunen, E. Hæggström, One kilometer (1 km) electric solar wind sail tether produced automatically, Review of Scientific Instruments 84 (2013) 095102, doi: 10.1063/1.4819795.

[8] S. Wagner, J. Sundqvist, G. Thornell, D41.2, Design description of the Remote Unit, Tech. rep., ESAIL FP7 project (2012).
URL `http://www.electric-sailing.fi/fp7/docs/D412.pdf`

[9] A. Kestilä, T. Tikka, P. Peitso, J. Rantanen, A. Näsilä, K. Nordling, H. Saari, R. Vainio, P. Janhunen, J. Praks, M. Hallikainen, Aalto-1 nanosatellite – technical description and mission objectives, Geoscientific Instrumentation, Methods and Data Systems 2 (2013) 121–130, doi: 10.5194/gi-2-121-2013.

[10] J. L. Wright, Space Sailing, Gordon and Breach Science Publisher, Berlin, 1992, pp. 42–45, ISBN: 2-88124-842-X.

[11] G. W. Hughes, C. R. McInnes, Small-body encounters using solar sail propulsion, Journal of Spacecraft and Rockets 41 (1) (2004) 140–150, doi: 10.2514/1.9277.

[12] P. Toivanen, P. Janhunen, Spin plane control and thrust vectoring of electric solar wind sail, Journal of Propulsion and Power 29 (1) (2013) 178–185, doi: 10.2514/1.B34330.

[13] G. Mengali, A. A. Quarta, P. Janhunen, Electric sail performance analysis, Journal of Spacecraft and Rockets 45 (1) (2008) 122–129, doi: 10.2514/1.31769.

[14] A. A. Quarta, G. Mengali, Electric sail mission analysis for outer solar system exploration, Journal of Guidance, Control, and Dynamics 33 (3) (2010) 740–755, doi: 10.2514/1.47006.

[15] G. Mengali, A. A. Quarta, Rapid solar sail rendezvous missions to asteroid 99942 Apophis, Journal of Spacecraft and Rockets 46 (1) (2009) 134–140, doi: 10.2514/1.37141.

[16] J. Rodríguez Canabal, J. M. Sánchez Pérez, A. Yáñez Otero, Rosetta: Consolidated report on mission analysis Churyumov-Gerasimenko 2004, Tech. Rep. RO-ESC-RP-5500, European Space

Agency, Robert-Bosch-Str. 5, D-64293 Darmstadt (Germany) (August 2003).

[17] C. R. McInnes, Solar Sailing: Technology, Dynamics and Mission Applications, Springer-Praxis Series in Space Science and Technology, Springer-Verlag, Berlin, 1999, pp. 13–14.

[18] P. Janhunen, A. A. Quarta, G. Mengali, Electric solar wind sail mass budget model, Geoscientific Instrumentation, Methods and Data Systems 2 (1) (2013) 85–95, doi: 10.5194/gi-2-85-2013.

[19] K. H. Glassmeier, et al., The Rosetta mission: Flying towards the origin of the solar system, Space Science Reviews 128 (2007) 1–21, doi: 10.1007/s11214-006-9140-8.

[20] B. Dachwald, H. Boehnhardt, U. Broj, U. Geppert, J. Grundmann, W. Seboldt, P. Seefeldt, P. Spietz, L. Johnson, E. Kührt, S. Mottola, M. Macdonald, C. R. McInnes, M. Vasile, R. Reinhard, Gossamer roadmap technology reference study for a multiple NEO rendezvous mission, in: M. Macdonald (Ed.), Advances in Solar Sailing, Springer Praxis Books, Springer Berlin Heidelberg, 2014, pp. 211–226.

List of Tables

	Earth	Comet 67P
a [au]	1.000000920477849	3.463049865528343
e	$1.667259177730655 \times 10^{-2}$	$6.410189001180967 \times 10^{-1}$
i [deg]	$1.862063137086164 \times 10^{-3}$	7.040450026522257
ω [deg]	$2.874007612074662 \times 10^{2}$	$1.277996164427588 \times 10^{1}$
Ω [deg]	$1.756254311917600 \times 10^{2}$	$5.014697961599386 \times 10^{1}$
M [deg]	$2.151682696364959 \times 10^{2}$	$3.03710525763619 \times 10^{2}$

Table 1
Orbital elements of the comet 67P and the Earth+Moon barycenter at 10 August 2014 (MJD = 56879).

a_c [mm/s^2]	ν_i [deg]	ν_f [deg]	r_f [au]	Δt [days]	n
0.15	208.17	142.38	4.14	4409	5
0.16	244.94	139.65	3.98	4057	5
0.17	178.56	148.07	4.47	3986	5
0.18	214.05	140.58	4.04	3553	4
0.19	244.57	138.29	3.91	3317	4
0.20	270.58	137.20	3.85	3149	4
0.21	294.75	136.60	3.81	3012	4
0.22	208.74	139.40	3.97	2805	4
0.23	234.49	136.89	3.83	2631	3
0.24	256.15	135.58	3.76	2507	3
0.25	274.85	134.80	3.72	2407	3
0.26	292.07	134.27	3.69	2320	3
0.27	309.15	133.87	3.67	2242	3
0.28	191.49	140.76	4.05	2125	3
0.29	214.28	135.98	3.78	1980	2
0.30	233.56	133.79	3.66	1882	2
0.31	249.16	132.47	3.59	1807	2
0.32	262.68	131.60	3.55	1745	2
0.33	274.68	130.96	3.51	1690	2
0.34	285.65	130.44	3.49	1641	2
0.35	295.97	129.99	3.46	1596	2
0.36	305.94	129.60	3.44	1554	2
0.37	315.83	129.23	3.43	1514	2
0.38	325.94	128.90	3.41	1477	2
0.39	336.67	128.60	3.40	1440	2
0.40	191.46	140.40	4.03	1357	1
0.45	247.64	126.39	3.29	1085	1
0.50	283.86	122.96	3.13	962	1
0.55	309.91	121.09	3.04	873	1
0.60	332.04	119.65	2.98	801	1
0.65	352.77	118.45	2.93	739	1
0.70	217.82	139.30	3.96	651	0
0.75	229.69	133.62	3.65	552	0
0.80	238.15	128.33	3.38	479	0
0.85	244.02	123.35	3.15	424	0
0.90	247.78	118.79	2.95	383	0
0.95	249.44	114.89	2.79	355	0
1	249.57	112.18	2.69	340	0

Table 2
Optimal transfer performance in an ephemeris-free model.

payload mass [kg]	a_c[mm/s^2]	flight time [years]	$\ell_{\rm tot}$[km]	m[kg]	N	$\ell_{\rm tether}$[km]
265	0.2	8.6	242	701	24	10.1
	0.4	3.7	506	733	36	14.1
	1.0	0.9	1412	819	60	23.5
165	0.2	8.6	154	446	20	7.7
	0.4	3.7	325	470	28	11.6
	1.0	0.9	919	533	48	19.1
30	0.2	8.6	33	96	8	4.1
	0.4	3.7	73	105	12	6.1
	1.0	0.9	225	130	24	9.4

Table 3
Spacecraft main parameters for some representative mission scenarios.

List of Figures

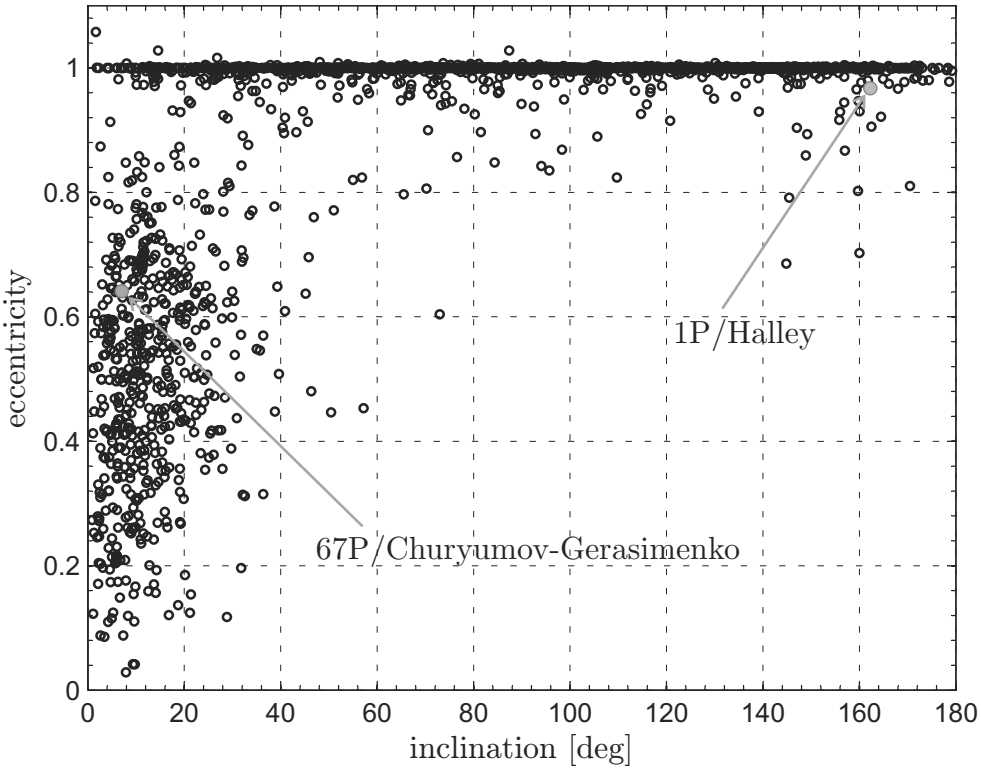

Figure 1. Orbital eccentricity as a function of the orbital inclination for the set of comets contained in the JPL's small-body database.

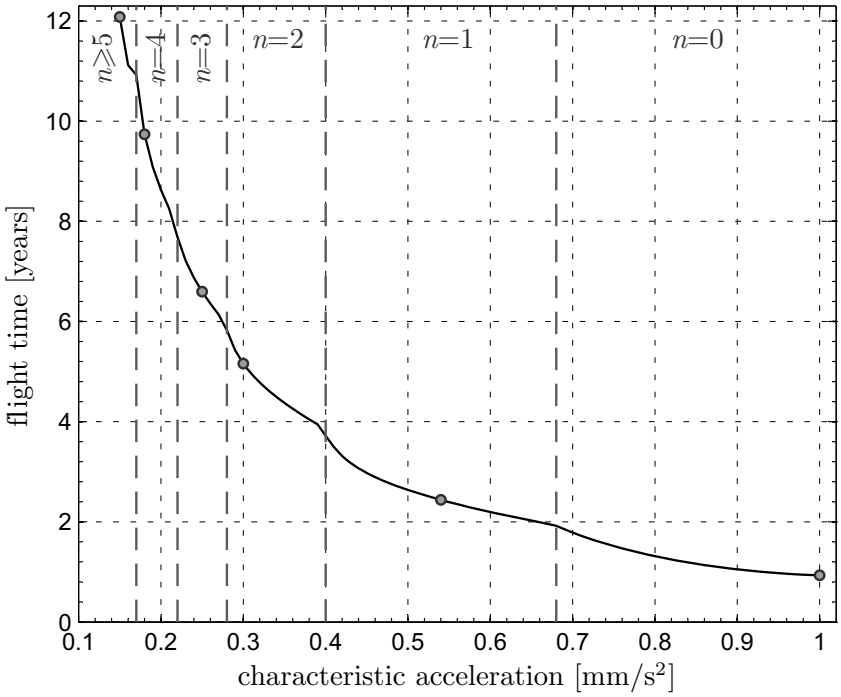

Figure 2. Minimum flight time as a function of the spacecraft characteristic acceleration in an ephemeris-free model. The circles correspond to the trajectories illustrated in Fig. 4.

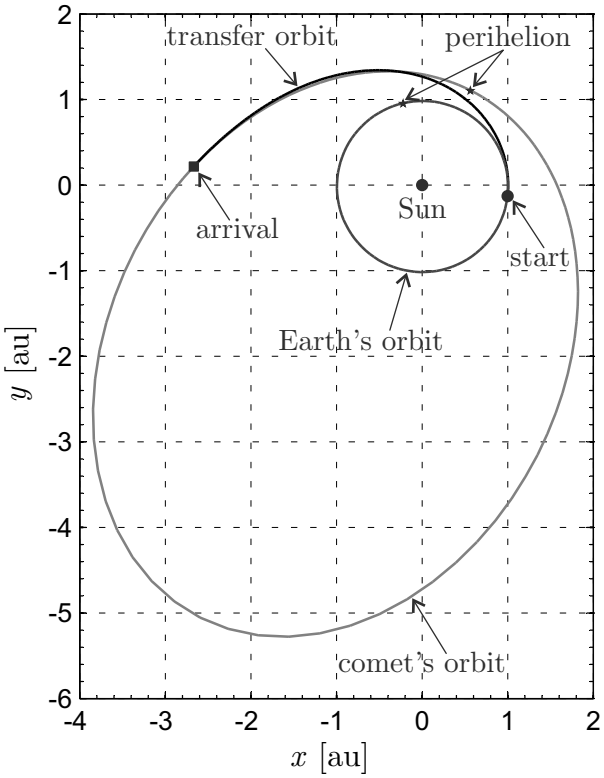

Figure 3. Optimal transfer orbit when $a_c = 1$ mm/s^2 in an ephemeris-free model (ecliptic projection).

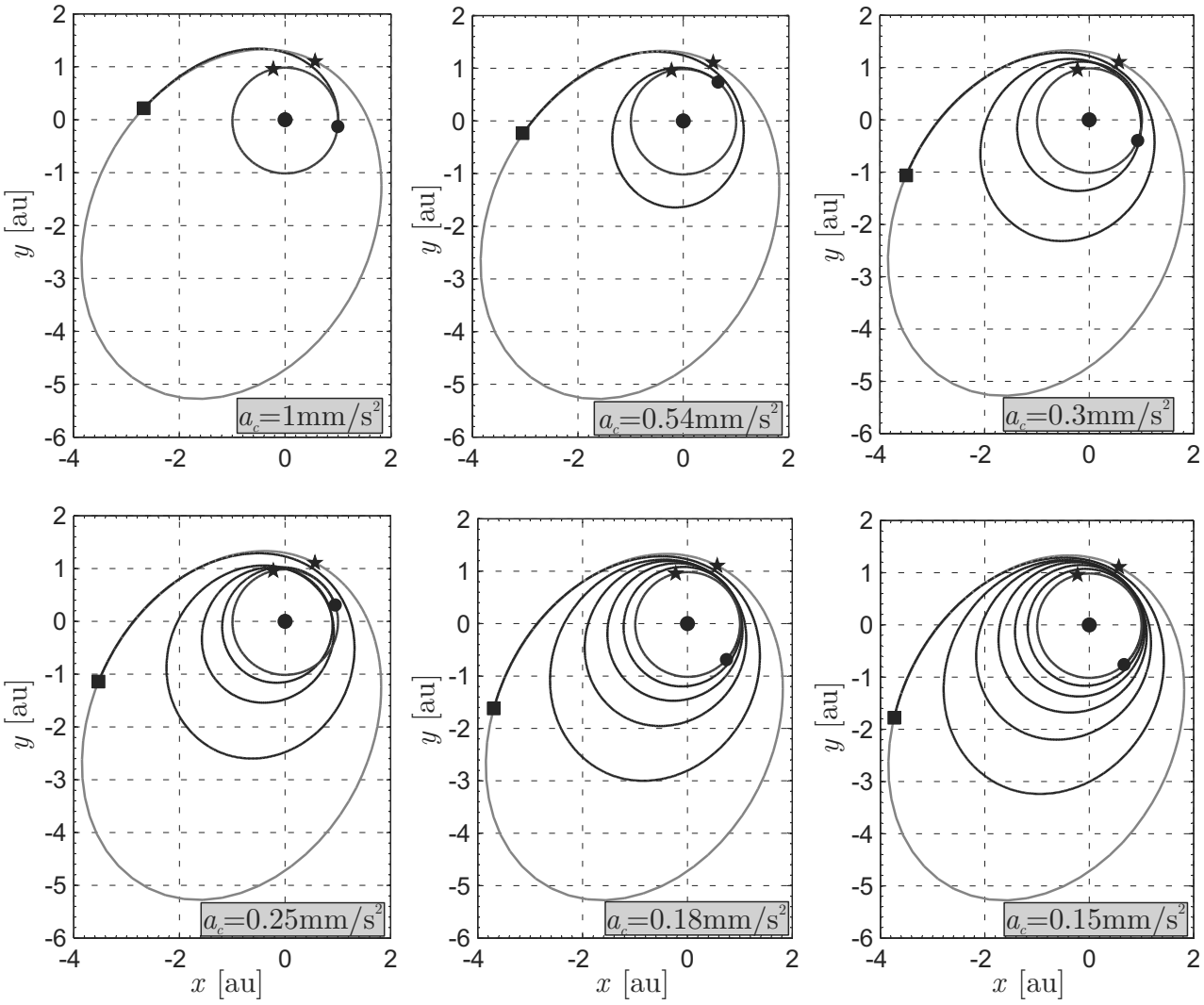

Figure 4. Optimal transfer orbits in an ephemeris-free model for some values of a_c (ecliptic projection).

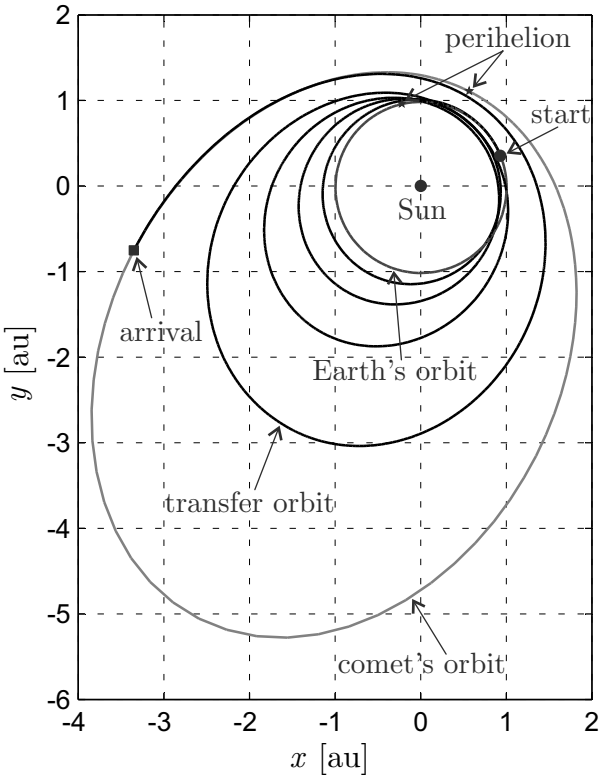

Figure 5. Optimal transfer trajectory when $a_c = 0.2$ mm/s^2, departure date 14 October 2020 (ecliptic projection).

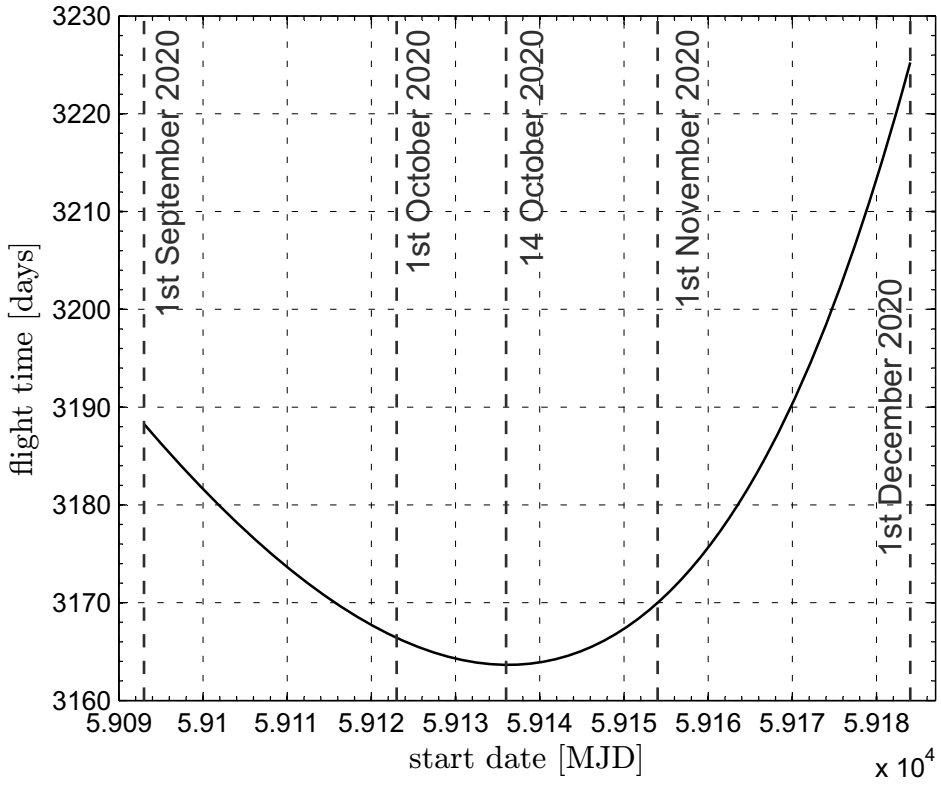

Figure 6. Minimum flight time as a function of the departure date when $a_c = 0.2$ mm/s^2.

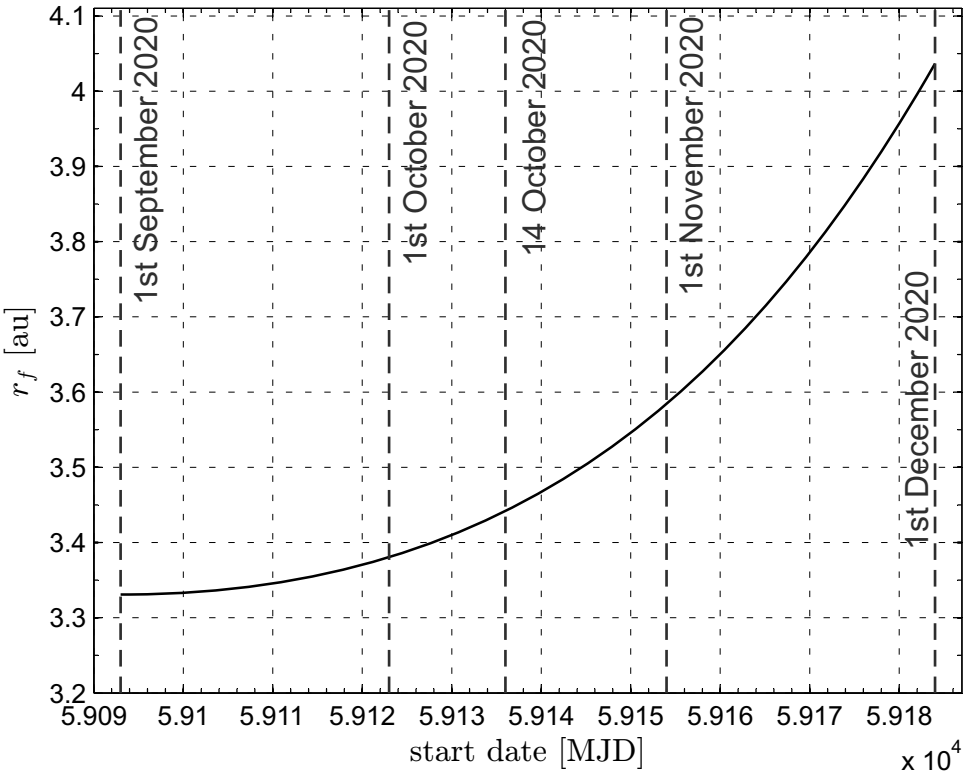

Figure 7. Sun-spacecraft distance at rendezvous as a function of the departure date when $a_c = 0.2$ mm/s^2.

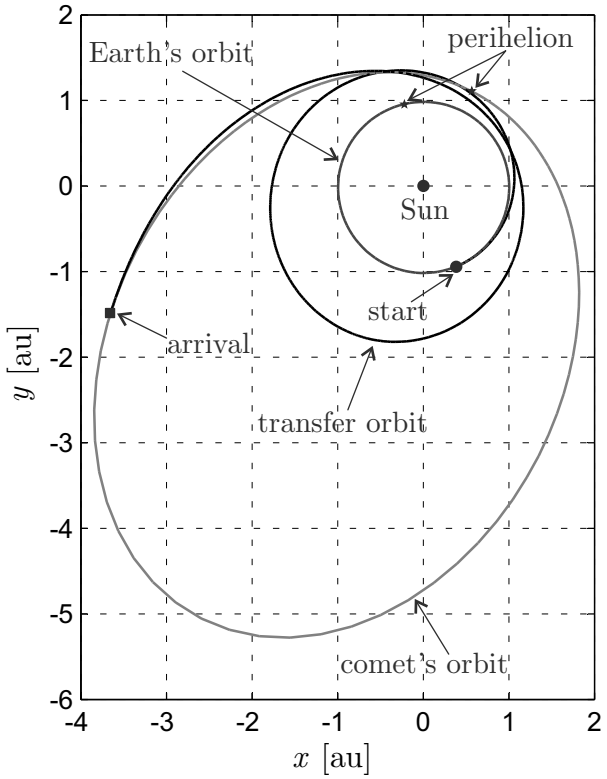

Figure 8. Optimal transfer trajectory when $a_c = 0.4$ mm/s^2, departure date 15 July 2019 (ecliptic projection).

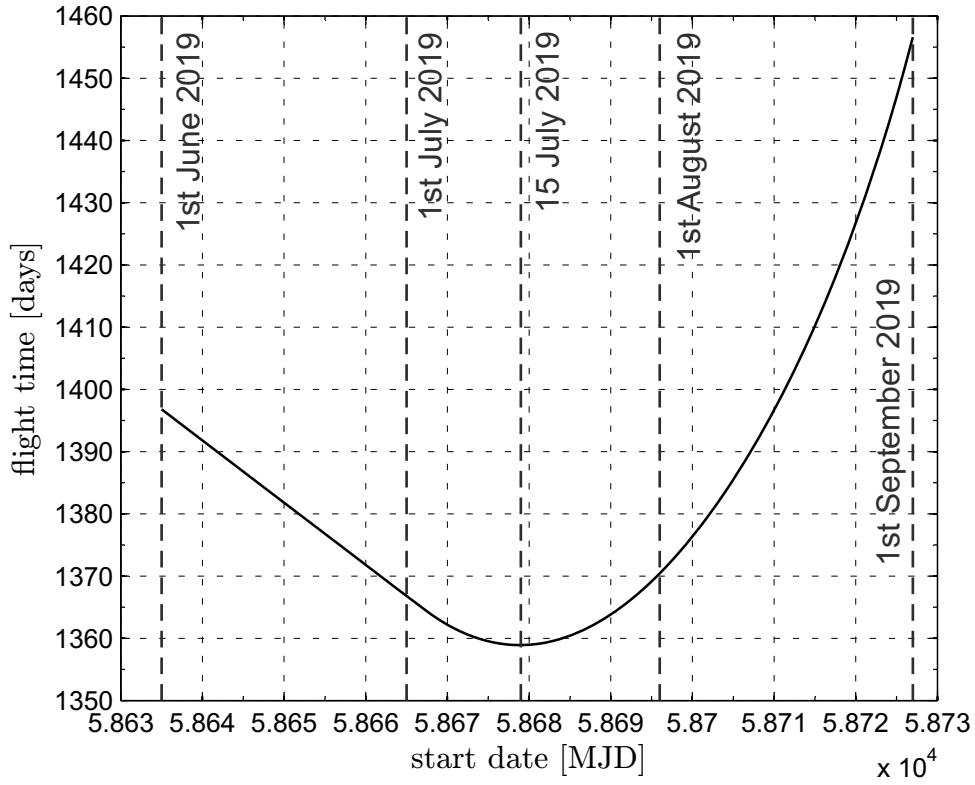

Figure 9. Minimum transfer time as a function of the departure date when $a_c = 0.4$ mm/s^2.

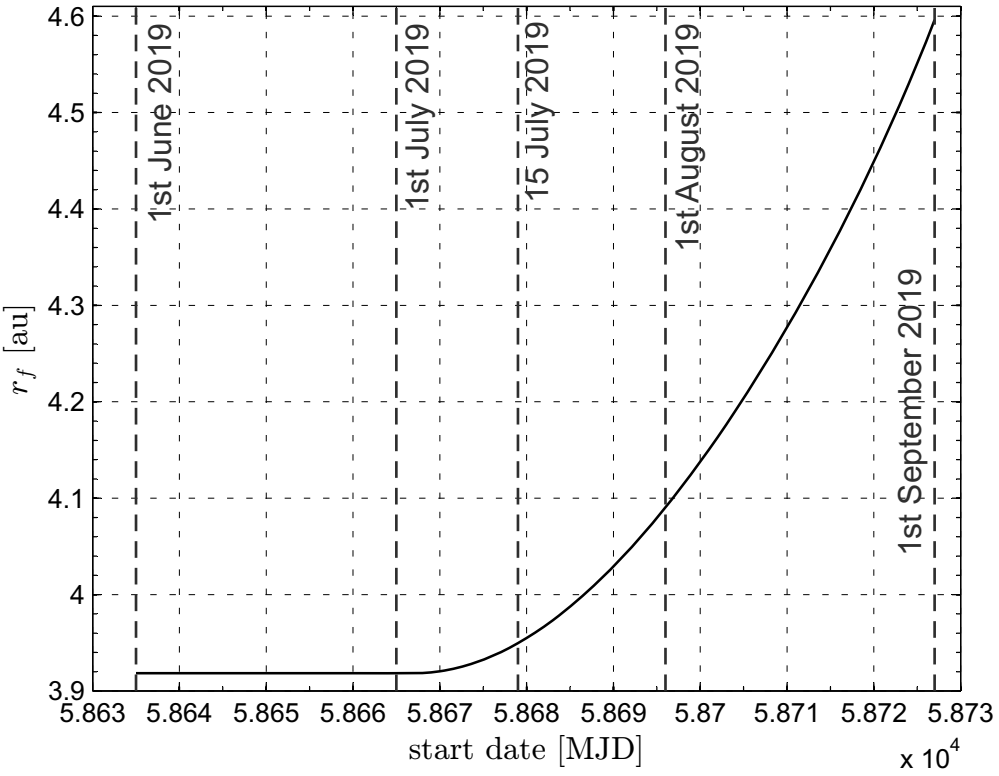

Figure 10. Sun-spacecraft distance at rendezvous as a function of the departure date when $a_c = 0.4$ mm/s^2.

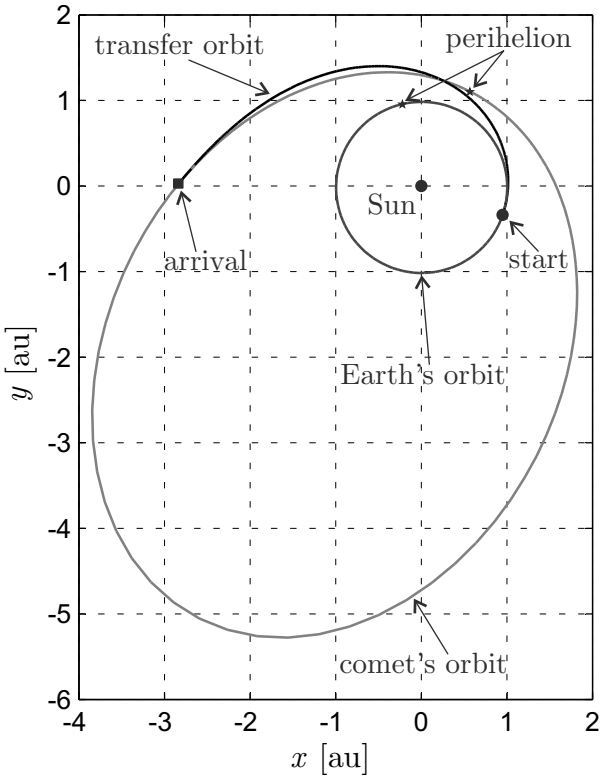

Figure 11. Optimal transfer trajectory when $a_c = 1$ mm/s^2, departure date 3 September 2021 (ecliptic projection).

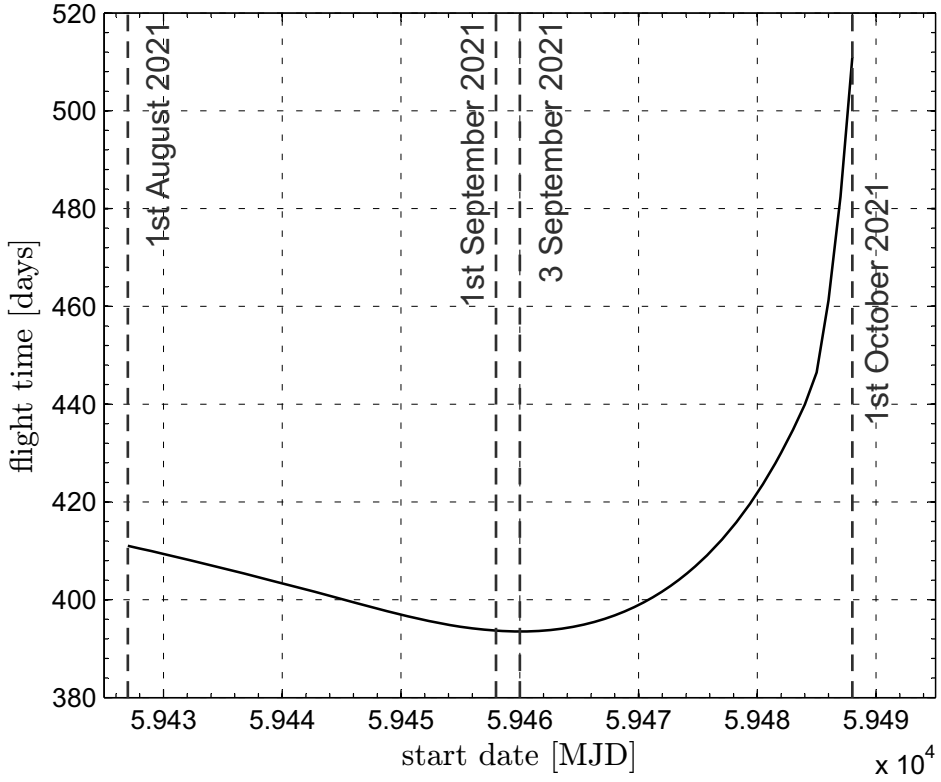

Figure 12. Minimum transfer time as a function of the departure date when $a_c = 1$ mm/s^2.

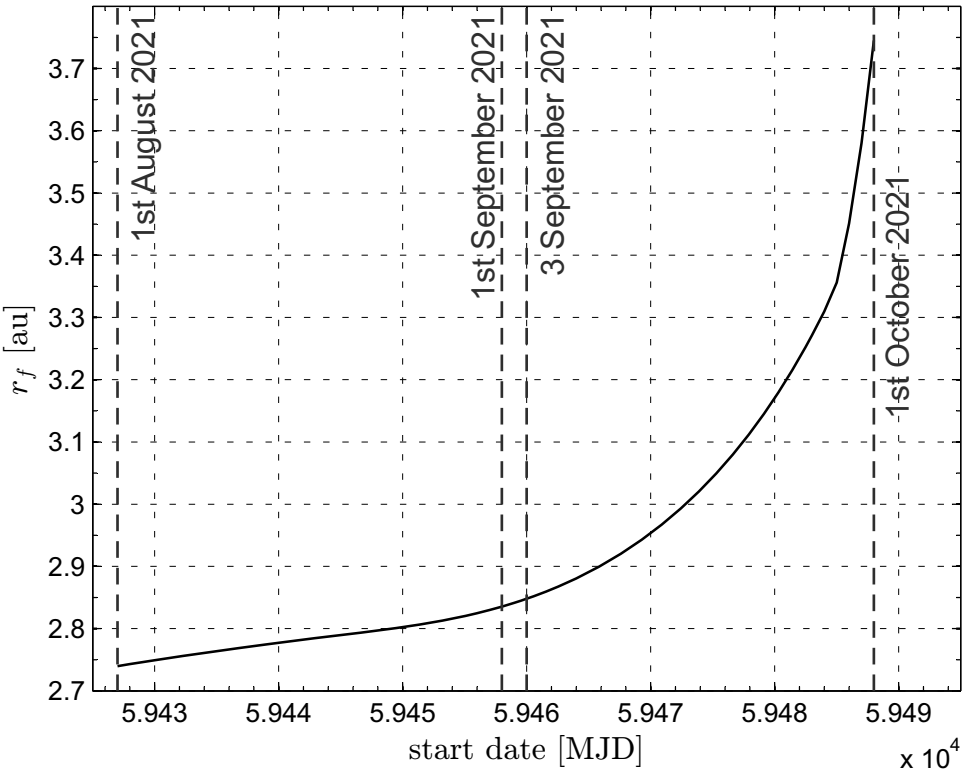

Figure 13. Sun-spacecraft distance at rendezvous as a function of the departure date when $a_c = 1$ mm/s^2.